Applied Catalysis B: Environmental 188 (2016) 13–22

Contents lists available at ScienceDirect

Applied Catalysis B: Environmental

journal homepage: www.elsevier.com/locate/apcatb

MoS_2-graphene/$ZnIn_2S_4$ hierarchical microarchitectures with an electron transport bridge between light-harvesting semiconductor and cocatalyst: A highly efficient photocatalyst for solar hydrogen generation

Yong-Jun Yuan[a,*], Ji-Ren Tu[a], Zhi-Jun Ye[a], Da-Qin Chen[a,*], Bin Hu[b], Yan-Wei Huang[a], Ting-Ting Chen[a], Da-Peng Cao[c], Zhen-Tao Yu[b,*], Zhi-Gang Zou[b]

[a] College of Materials and Enviromental Engineering, Hangzhou Dianzi University, Hangzhou, Zhejiang 310018, China
[b] Jiangsu Provincial Key Laboratory for Nanotechnology, Collaborative Innovation Center of Advanced Microstructures, College of Engineering and Applied Science, Nanjing University, Nanjing, Jiangsu 210093, China
[c] College of Materials Science and Engineering, Nanjing University of Posts and Telecommunications, Nanjing, Jiangsu 210022, China

ARTICLE INFO

Article history:
Received 26 October 2015
Received in revised form 21 January 2016
Accepted 26 January 2016
Available online 29 January 2016

Keywords:
MoS_2-graphene/$ZnIn_2S_4$
Photocatalysis
Hierarchical microarchitectures
Solar hydrogen generation
Noble-metal-free

ABSTRACT

Exploiting photocatalysts with characteristics of cost effectiveness, environmental friendliness, visible light response, high reactivity and good durability is a great challenge for solar H_2 generation. Here, we synthesis of MoS_2-graphene composite as a highly-efficient cocatalyst to enhance the photocatalytic activity of $ZnIn_2S_4$ under visible light irradiation. Through the optimizing of each composition proportion, the hierarchical MoS_2-graphene/$ZnIn_2S_4$ photocatalyst shows the highest H_2 evolution rate of 4169 $\mu mol\, h^{-1}\, g^{-1}$ under visible light irradiation in presence of Na_2S and Na_2SO_3 as sacrificial reagents when the content of MoS_2-graphene is 1.2 wt% and the weight ratio of MoS_2 to graphene is 10:1, which is almost 22.8 times higher than that of pure $ZnIn_2S_4$. More importantly, the ternary MoS_2-graphene/$ZnIn_2S_4$ composite exhibits much higher photocatalytic activity than Pt-loaded $ZnIn_2S_4$ photocatalyst, suggesting that the MoS_2-graphene composite can act as a more efficient cocatalyst than the commonly used Pt metal. The superior catalytic activity of MoS_2-graphene cocatalyst can be assigned to the positive synergistic effect between MoS_2 and graphene, which act as a hydrogen evolution reaction catalyst and an electron transport bridge, respectively. The effective charge transfer from $ZnIn_2S_4$ to MoS_2 through graphene is demonstrated by the significant enhancement of photocurrent responses in MoS_2-graphene/$ZnIn_2S_4$ composite photoelectrodes.

1. Introduction

Utilization of solar energy to make hydrogen fuel via photocatalytic water splitting represents a promising solution to providing renewable and carbon-free energy needed for sustainable development [1–3]. Semiconductor-based photocatalyst, especially for highly active mesoporous TiO_2, which has been attracting extensive attention for solar H_2 generation in the past decades [4–6]. Unfortunately, TiO_2 is a wide band gap semiconductor, which responds only to ultraviolet light. In order to harvest more light, a great number of visible-light-responsive photocatalysts have been designed, prepared and investigated for heterogeneous photocatalytic hydrogen evolution system, such as Cu_2O [7], CdS [8–10], CdSe [11], $CuInS_2$ [12], Cu_2ZnSnS_4 [13], TaON [14,15], and g-C_3N_4 [16]. Unfortunately, these semiconductors have been limited by various factors including fast recombination of electron-hole pairs, poor stability, environmental unfriendliness and/or low activity. Therefore, exploiting more efficient and visible-light-responsive photocatalysts to meet the requirement of practical application is still a challenge in the photocatalysis field. In recent years, the ternary sulfide semiconductor of $ZnIn_2S_4$ is a promising candidate photocatalyst for solar hydrogen generation because of its suitable band gap (~2.40 eV) and considerable chemical stability [17,18]. However, the H_2 production activity of pure $ZnIn_2S_4$ is low because of its quick recombination of photogenerated electron-hole pairs. It is well known that suitable cocatalysts loaded on semiconductor photocatalysts act as active sites for hydrogen evo-

* Corresponding authors.
E-mail addresses: yjyuan@hdu.edu.cn (Y.-J. Yuan), dqchen@hdu.edu.cn (D.-Q. Chen), yuzt@nju.edu.cn (Z.-T. Yu).

http://dx.doi.org/10.1016/j.apcatb.2016.01.061
0926-3373/

lution reaction, which can decrease the overpotential of hydrogen evolution reaction. More importantly, the cocatalyst can suppress the recombination of photoexcited electron-hole pairs in semiconductor, resulting in a significant enhancement in the photocatalytic activity. To date, noble metal of Pt has been widely employed as a highly efficient cocatalyst to improve the photocatalytic H_2 evolution activity of $ZnIn_2S_4$ [19]. Unfortunately, the rareness and high cost of precious metal Pt hunder its application in solar-to-H_2 conversion. Hence, the exploitation of cocatalysts composed exclusively of low-cost and earth-abundant elements is highly desirable. Ye et al. have reported the enhanced photocatalytic H_2 evolution activity of $ZnIn_2S_4$ by incorporation of graphene as a cocatalyst. [20] They concluded that the graphene served as an electron acceptor and mediator, as well as the cocatalyst, resulted in the enhanced photocatalytic activity of $ZnIn_2S_4$. However, the H_2 production activity of system based on graphene/$ZnIn_2S_4$ photocatalyst must be further enhanced from the viewpoint of practical application.

Recently, Wei et al. have prepared MoS_2/$ZnIn_2S_4$ composite photocatalyst for solar H_2 generation, and the photocatalyst showed highly enhanced photocatalytic activity with the maximum H_2 evolution rate of 3060 $\mu mol\, h^{-1}\, g^{-1}$ under visible light irradiation [21]. In particular, the two-dimensional (2D) MoS_2 has been reported to be a highly efficient hydrogen evolution reaction catalyst for both electrochemical and photochemical water reduction owing to its excellent H_2 activation property of S atoms on the exposed edges [22–29]. Previous studies have suggested that layered MoS_2 is a more effective cocatalyst than many noble metals, such as Ru, Pt, Rh, Ir, and Pd [30–32]. However, the poor electrical conductivity of MoS_2 still restricts the overall hydrogen evolution reaction activity. Previous studies have shown that the two-dimensional (2D) graphene has larger surface area and high electron conductivity, the introduction of graphene on the surface of semiconductor photocatalysts not only provides larger specific surface area for cocatalyst dispersion, but also accelerates the interfacial electron transfer from light-harvesting semiconductor to cocatalyst [33,34]. Xiang et al. have reported a novel strategy to accelerate the transfer of photogenerated electrons from TiO_2 to MoS_2 by using graphene as an electron transport bridge [35]. The positive synergetic effect between MoS_2 and graphene was supposed to be the key factor for the enhanced photocatalytic activity. However, the MoS_2-graphene/TiO_2 photocatalyst was inactive under visible light irradiation owing to the wide band gap of TiO_2. Until recently, Chang and coworkers have prepared MoS_2-graphene modified CdS hybrid photocatalyst for solar H_2 generation, a high apparent quantum yield of 28.1% at 420 nm was obtained [36]. They concluded that the hybrid cocatalyst not only provides abundant reactive sites but also increases the transfer of charge carriers, resulted in the significantly improvement in the photocatalytic H_2 production activity. Unfortunately, cadmium is one of the most widespread environmental pollutants with high toxicity. Therefore, it is highly desirable to design and construct environmentally-friendly light-harvesting semiconductor to combine with MoS_2-graphene cocatalyst for robust and efficient solar H_2 generation system. Accord to our knowledge, no previous study regarding the application of a MoS_2-graphene/$ZnInS_2$ hybrid photocatalyst with the MoS_2-graphene composite as the cocatalyst for H_2 production has been reported to date.

In this study, for the first we report the synthesis of hierarchical MoS_2-graphene/$ZnInS_2$ composite photocatalyst by a hydrothermal method for solar H_2 generation in Na_2S-Na_2SO_3 solution under visible light irradiation. The consequences show that the activity of the $ZnIn_2S_4$ can be significantly enhanced by loading of MoS_2-graphene cocatalyst, and the MoS_2-graphene/$ZnIn_2S_4$ photocatalyst shows a much higher H_2 evolution rate than those of Pt/$ZnIn_2S_4$ and MoS_2/$ZnIn_2S_4$ under the same test conditions. This study will prove new insight into designing and developing of visible-light-responding, environmentally-friendly, noble-metal-free, highly-reactive and stable photocatalysts for solar H_2 generation.

2. Experimental

2.1. Chemicals

Regents. Zinc chloride ($ZnCl_2$), indium trichloride ($InCl_3$), sodium molybdate dehydrate ($Na_2MoO_4{\cdot}2H_2O$) and thioacetamide (CH_3CSNH_2) were purchased from Alfa Aesar China (Tianjin) Co., Ltd. Graphene oxide (GO, 99%) was purchased from Jichang nanotechnology (Nanjing) Co., Ltd.

2.2. Instrumentation

The X-ray diffraction (XRD) patterns of all samples were taken on a Bruker D8 Advance X-ray diffractometer (Cu Kα, λ = 0.15406 nm, 40 kV and 40 mA, Germany) in the range of 10–80° with a scan speed of 5° min^{-1}. UV–vis diffuse reflectance spectra (UV–vis DRS) of samples were analyzed by using a UV–vis spectrophotometer (Varian cary 500, American), in which $BaSO_4$ was used as the background. The morphologies of photocatalysts were obtained on field emission scanning electron microscopic (FESEM, vltra55, a Carl Zeiss Gemini) and high resolution transmission electron microscopy (HRTEM, JEOL JEM 2010). All SEM samples were created by depositing a drop of diluted suspensions in ethanol on a silicon chip. All TEM samples were obtained by depositing a drop of diluted suspensions in ethanol on a carbon-film-coated copper grid and naturally dried. The chemical composition of photocatalysts was analyzed with X-ray photoelectron spectroscopy (XPS) analysis on a VG ESCALAB MKII XPS system using Al Kα X-ray as the excitation source. All the binding energies were calibrated using the C1s peak at 284.8 eV. The photocurrent curves of samples were recorded in a conventional three-electrode configuration using an electrochemical analyzer (CHI-B600, Changhua, China). The Pt wire, Ag/AgCl and as-prepared photoelectrode were used as the counter electrode, reference electrode and working electrodes, respectively. The photocurrent curves were measured in 0.5 M Na_2SO_4 aqueous solution with a 300 W Xenon lamp equiped with a cutoff filter (λ > 420 nm) as the light source. The photoluminescence spectra were measured on an Edinburgh FS5 spectrofluorometer.

2.3. Preparation and characterization

2.3.1. MoS_2-graphene cocatalyst

The MoS_2-graphene composites were prepared by hydrothermal reaction of graphene oxide in an aqueous solution with $Na_2MoO_4{\cdot}2H_2O$ and thioacetamide. The nominal weight ratios of $Na_2MoO_4{\cdot}2H_2O$ to graphene oxide were 40:1, 20:1, 10:1, 1:1, 1:5 and 1:10, and the obtained powders were labeled as $Mo_{40}G_1$, $Mo_{20}G_1$, $Mo_{10}G_1$, Mo_1G_1, Mo_1G_5 and Mo_1G_{10}, respectively. In a typical synthesis of MoS_2-graphene composite, 5 mg of graphene oxide was dispersed in 40 mL of aqueous solution consisting of 50 mg $Na_2MoO_4{\cdot}2H_2O$ and 200 mg thioacetamide to form a transparent solution. The mixed solution was then transferred into a 50 mL Teflon-lined stainless steel autoclave and then treated at 210 °C for 24 h in an electric oven. The black precipitate was collected via centrifugation, and washed three times with deionized water and ethanol before drying at 80 °C for 12 h to obtain a $Mo_{10}G_1$ sample. The other MoS_2-graphene composites were synthesized by changing the ratio of $Na_2MoO_4{\cdot}2H_2O$ to graphene oxide with the same method. For comparison, pure MoS_2 and graphene samples were prepared through the same procedure by using thioacetamide as a reductant.

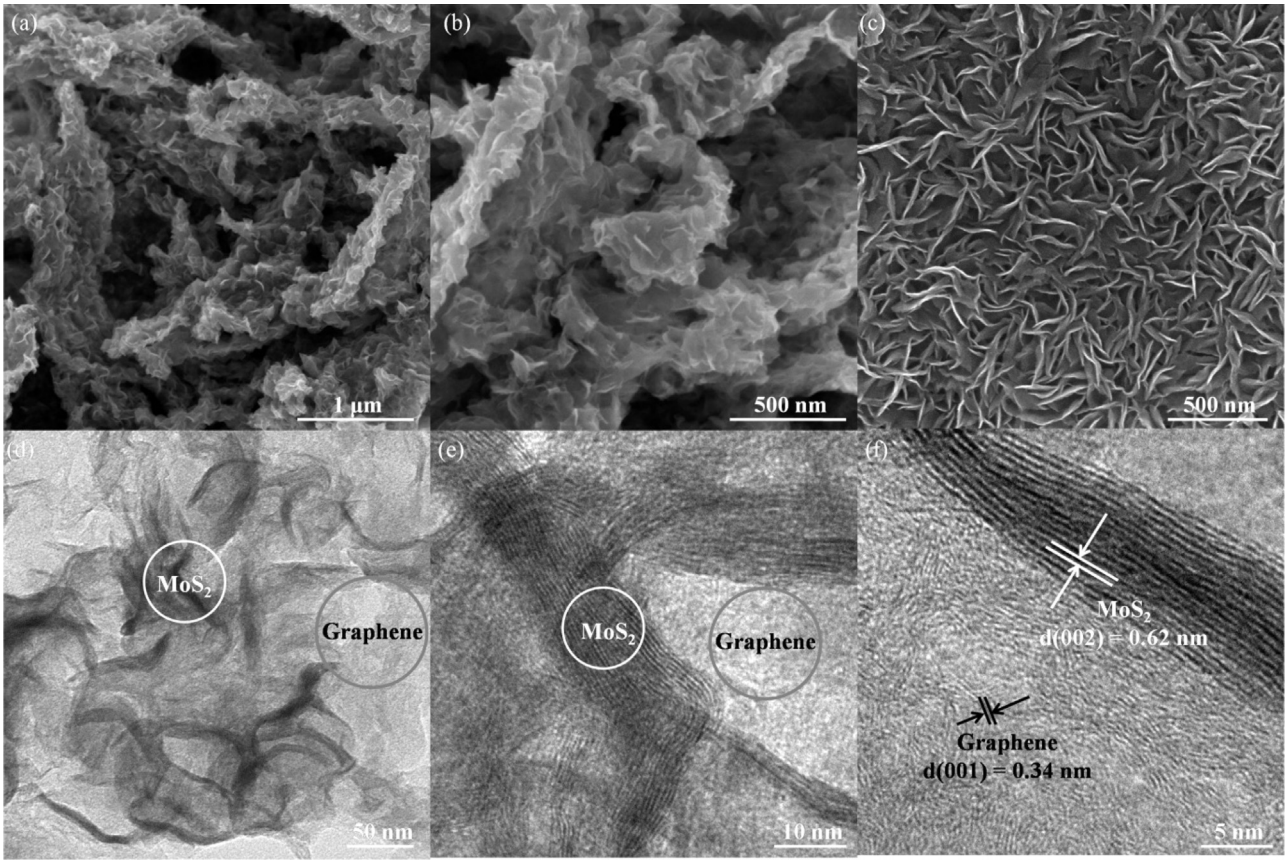

Fig. 1. (a) and (b) SEM images of MoS_2-graphene composite cocatalyst; (c) SEM image of pure MoS_2 nanosheets; (d–f) TEM images of MoS_2-graphene composite cocatalyst.

2.3.2. MoS_2-graphene/$ZnIn_2S_4$ photocatalysts

Typically, $ZnCl_2$ (0.136 g, 1 mmol) and $InCl_3$ (0.442 g, 2 mmol), thioacetamide (TAA, 0.3 g, 4 mmol) and MoS_2-graphene (4 mg) were dispersed in 40 mL deionized water under vigorous stirring and the suspension continued to ultrasonicate for a few minutes. After that, the mixture solution was transferred into a 50 mL Teflon-lined stainless steel autoclave, which was then heated at 200 °C in an electric oven for 24 h. After the autoclave was cooled naturally to room temperature, the produced yellow powder was collected via centrifugation, followed by washing with ethanol and distilled water for several times and drying at 80 °C for 12 h. Finally, the obtained MoS_2-graphene/$ZnIn_2S_4$ composite was annealed at 350 °C for 4 h in the atmosphere of nitrogen. For comparison, the pure $ZnIn_2S_4$ was also prepared by the above-mentioned method in absence of MoS_2-graphene composite. Besides, the MoS_2/$ZnIn_2S_4$ and graphene/$ZnIn_2S_4$ composites were also prepared by a similar hydrothermal reaction in presence of MoS_2 or graphene alone, respectively. The thin film of MoS_2-graphene/$ZnIn_2S_4$ was prepared by coating 0.2 mL of 5 mg mL^{-1} solution on an ITO glass, which was then heated at 300 °C under nitrogen atmosphere.

2.4. Photocatalytic H_2 production

Photocatalytic H_2 production reactions were carried out in a sealed Pyrex top-irradiation reaction vessel with a capacity of 150 mL. A 300 W xenon lamp equipped with a cut-off filter ($\lambda > 420$ nm) was used to provide the visible light irradiation. In a typical photocatalytic H_2-evolution experiment, 50 mg H_2-evolving photocatalyst was dispersed in a 50 mL aqueous solution containing 0.25 M Na_2SO_3 and 0.25 M Na_2S as sacrificial reagents. Before irradiation, the reaction solution was evacuated and purged argon several times to completely remove air. The amount of evolved H_2 was determined with a gas chromatograph (JieDao, GC1609, MS-5A column, TCD, Ar carrier). Typically, 1 mL of gas sample was intermittently extracted from the reaction vessel and injected into the gas chromatograph, and the amount of H_2 was calculated according to the fitted standard curve. The Pt nanoparticles were loaded on the surface of $ZnIn_2S_4$ *in-situ* by photoreduction method using H_2PtCl_6 as the precursor.

3. Results and discussion

3.1. Characterization of MoS_2-graphene/$ZnIn_2S_4$ photocatalysts

The MoS_2-graphene/$ZnIn_2S_4$ photocatalysts were prepared by a two-step hydrothermal process, and the overall synthetic procedure is shown schematically in Fig. S1 (Supporting information). In the first step, the layered MoS_2/graphene composite was prepared by hydrothermal reaction of graphene oxide with Na_2MoO_4 and CH_3CSNH_2 according to a previously reported method [35]. Fig. 1a and b shows the field emission scanning electron microscopic (FESEM) images of MoS_2/graphene composite, in which the MoS_2 nanosheets was deposited on graphene surface uniformly with a diameter of 200–250 nm. Notably, the MoS_2/graphene composite exhibits similar morphology behaviour as that of pure MoS_2 nanosheets shown in Fig. 1c. To better investigate the interfacial structure of MoS_2/graphene cocatalyst, the obtained MoS_2/graphene composite was further studied by the transmission electron microscopy (TEM). As shown in Fig. 1d, the TEM image shows that flower-like MoS_2 nanosheets were deposited on the graphene with a typical 2D structure. Such a 2D construction of MoS_2/graphene composite cocatalyst is supposed to has more active sites for hydrogen evolution reaction. The high resolution transmission electron microscopy (HRTEM) image of

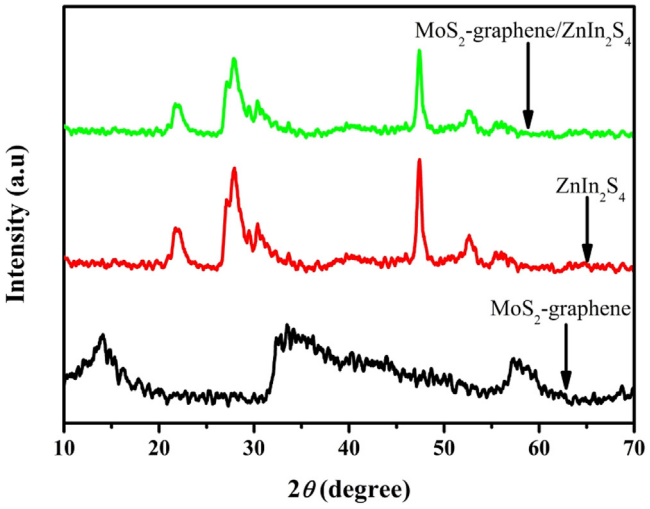

Fig. 2. XRD patterns of $ZnIn_2S_4$ alone, 1.2 wt% MoS_2-graphene and 1.2 wt% $Mo_{10}G_1/ZnIn_2S_4$ composite.

MoS_2/graphene cocatalyst illustrated in Fig. 1e shows the numbers of MoS_2 layers exhibited in the MoS_2/graphene cocatalyst is approximately 16. The lattice fringes of ca. 0. 34 and 0.62 nm were very clearly in the HRTEM image (Fig. 1f), which can be assigned to the (0 0 1) and (0 0 2) planes of graphene and hexagonal MoS_2, respectively [37,38]. After subsequent hydrothermal treatment of $ZnCl_2$, $InCl_3$ and CH_3CSNH_2 in an aqueous solution of the as-prepared MoS_2/graphene cocatalyst at 200 °C for 24 h led to the formation of three-dimensional hierarchical MoS_2/graphene-$ZnIn_2S_4$ photocatalyst.

The crystallinity and the phase of as-prepared $ZnIn_2S_4$ alone, MoS_2/graphene and MoS_2/graphene-$ZnIn_2S_4$ composites were investigated by powder X-ray diffraction (XRD) pattern. As shown in Fig. 2, the pure $ZnIn_2S_4$ sample shows six main diffraction peaks appeared at $2\theta = 21.74°$, 28.02°, 39.82°, 47.30°, 52.72° and 55.73°, which can be attributed to the (0 0 6), (1 0 2), (1 0 8), (1 1 0), (1 1 6) and (0 2 2) lattice plane of the hexagonal $ZnIn_2S_4$ (JCPDS card No. 03-065-2023), respectively [20,21]. As for the MoS_2/graphene cocatalyst, the three broad peaks observed at $2\theta = 13.94°$, 33.36° and 57.53 ° correspond respectively to the (0 0 2), (1 0 0) and (1 1 0) planes of the hexagonal MoS_2 (Fig. S2, JCPDS card No. 87-2416) [39]. It is worth noting that no diffraction peak of graphene was observed in XRD pattern of MoS_2/graphene cocatalyst, which could be assigned to the low diffraction intensity of graphene [36]. Furthermore, it is obvious that the as-prepared MoS_2/graphene-$ZnIn_2S_4$ photocatalyst is mainly composed of $ZnIn_2S_4$ and shows no diffraction peak of either MoS_2 or graphene component, probably due to the small amount of MoS_2/graphene content and its high dispersion on the surface of $ZnIn_2S_4$. However, the MoS_2 and graphene components in MoS_2/graphene-$ZnIn_2S_4$ composite photocatalyst can be confirmed by the following HRTEM and XPS analysis, as discussed later.

The microstructures of synthesized hierarchical MoS_2/graphene-$ZnIn_2S_4$ composite photocatalyst were then investigated by SEM and TEM. As shown in Fig. 3a and b, the SEM images reveal that the MoS_2/graphene-$ZnIn_2S_4$ composite was made up of microspheres with dimension in range of 3–4 μm assembled by densely flower-like nanoshheets. Similar observation was also obtained from the TEM image shown in Fig. 3c. The SEM and TEM images show a hierarchical architecture of the as-prepared MoS_2/graphene-$ZnIn_2S_4$ composite. Holes can be clearly seen in the MoS_2/graphene-$ZnIn_2S_4$ microspheres, suggesting that these microspheres have a hollow interior. After incorporation of MoS_2/graphene cocatalyst, the MoS_2/graphene-$ZnIn_2S_4$ composite has similar morphology with that of pure $ZnIn_2S_4$ (Fig. S3). The average diameter of MoS_2/graphene-$ZnIn_2S_4$ composite shows no apparent change, indicating that the MoS_2/graphene added does not affect the growth of $ZnIn_2S_4$. Furthermore, the HRTEM image illustrated in Fig. 3d clearly show that the composite is made up of $ZnIn_2S_4$, graphene and MoS_2, and the MoS_2/graphene cocatalyst was dispersed intimately on $ZnIn_2S_4$ surface. More importantly, the intimate interfaces between the $ZnIn_2S_4$ and MoS_2/graphene favor the photogenerated charge carrier transfer from $ZnIn_2S_4$ to MoS_2 through the graphene component, which could be a key factor in determining the photocatalytic H_2 production activity of MoS_2/graphene-$ZnIn_2S_4$ photocatalyst. The lattice fringes of 0.32, 0.34 and 0.62 nm can be attributed to the (1 0 2), (0 0 1) and (0 0 2) plane of $ZnIn_2S_4$, graphene and MoS_2, respectively [20,35]. In fact, it is different to synthesize the composite with graphene just at the intermediate of MoS_2 and $ZnIn_2S_4$. For MoS_2-graphene loaded semiconductor photocatalysts, the MoS_2 component could be located between graphene and light-harvesting semiconductor [35,36].

To characterize the chemical composition of as-prepared MoS_2/graphene-$ZnIn_2S_4$ photocatalyst, X-ray photoelectron spectroscopy (XPS) measurement was used to determine the exact surface state. As shown in Fig. 4a, the full-range XPS spectra of MoS_2/graphene-$ZnIn_2S_4$ photocatalyst shows the binding energy peaks at 162.2, 226.1, 288.2, 445.1, 532.1 and 1022.8 eV, which can be attributed to the S 2p, Mo 3d, C 1s, In 3d, O 1s and Zn 2p peaks, respectively [40–42]. Fig. 4b shows the high-resolution XPS spectra of Zn 2p, which contains Zn $2p_{3/2}$ at 1022.8 eV and Zn $2p_{1/2}$ at 1045.3 eV. In addition, the doublet peaks for In 3d at 444.8 and 452.1 eV illustrated in Fig. 4c, which can be assigned to In $3d_{5/2}$ and In $3d_{3/2}$, respectively. The XPS spectrum in the Mo 3d region exhibits binding energy at 228.8 eV for Mo $3d_{5/2}$ and 231.9 eV for Mo $3d_{3/2}$ (Fig. 4d), indicating that the Mo element exbits in the chemical formation of Mo^{4+}. As illustrated in Fig. 4e, the appearance of S $2p_{3/2}$ and S $2p_{1/2}$ peaks at 161.7 and 162.8 eV, which can be assigned to the S^{2-} in $ZnIn_2S_4$ and MoS_2. As compared to the binding energy of Zn 2p (1020.7 and 1043.6 eV) and In 3d (443.3 and 450.9 eV) of pure $ZnIn_2S_4$ illustrated in Fig. S4, a higher binding energy shift was observed could be attributed to the strong interaction between $ZnIn_2S_4$ and MoS_2/graphene cocatalyst. Fig. 4f shows the binding energy of C1s ranged from 282 to 290 eV, and the spectra contains peaks at 284.6, 285.6, 286.5, 287.5 and 288.9 attributable to the C—N, C—C, C—O, C=O and O—C=O, respectively [43].

The UV–vis absorption spectra of $ZnIn_2S_4$, graphene/$ZnIn_2S_4$, MoS_2/$ZnIn_2S_4$ and MoS_2/graphene-$ZnIn_2S_4$, are compared in Fig. 5a. All the samples have the similar absorption spectra. The pure $ZnIn_2S_4$ has a strong absorption in visible light region with an absorption edge at 528 nm, corresponding to a band gap of 2.39 eV. After addition of graphene, MoS_2, or MoS_2/graphene composite, the enhanced absorption in the visible region is clearly observed compared to pure $ZnIn_2S_4$, which can be attributed to the light absorption of MoS_2 and graphene. It can be seen that the absorption intensity in visible light region increases with the increased amounts of MoS_2/graphene composite (Fig. 5b), which is in accordance with the color changing from yellow to sallow. It has been known that the transfer efficiency of photogenerated charge carriers from light-harvesting semiconductor to cocatalyst is one of the key factors in determining the over photocatalytic activity of photocatalyst [44]. It is well known that the photoluminescence (PL) emission mainly results from the recombination of free charge carriers, then a lower PL intensity indicates a lower recombination rate of excited electrons and holes [45]. In the present study, the PL emission spectra were used to investigate the efficiency of the interfacial electron transfer from $ZnIn_2S_4$ to MoS_2-RGO. Fig. 6a shows the comparison of PL emission spectra of pure

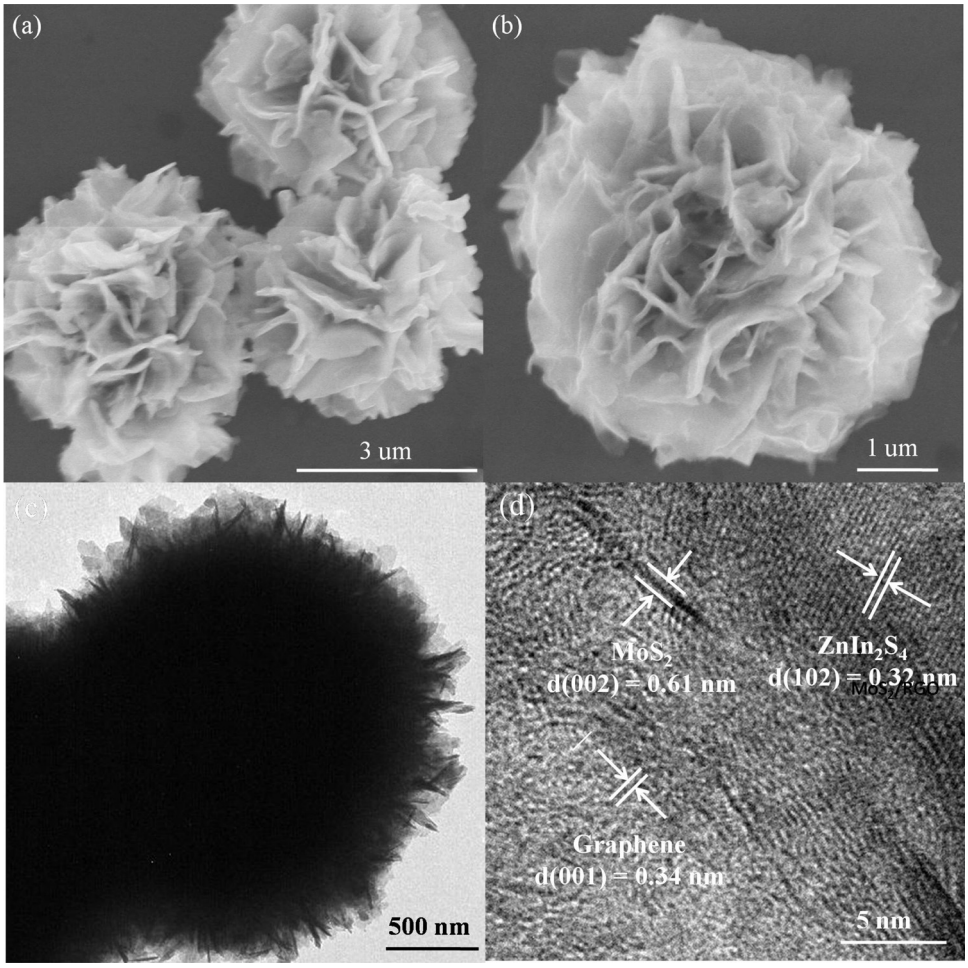

Fig. 3. (a) and (b) SEM images of 1.2 wt% $Mo_{10}G_1/ZnIn_2S_4$ composites; (c) TEM and (d) HRTEM images of 1.2 wt% $Mo_{10}G_1/ZnIn_2S_4$ composite.

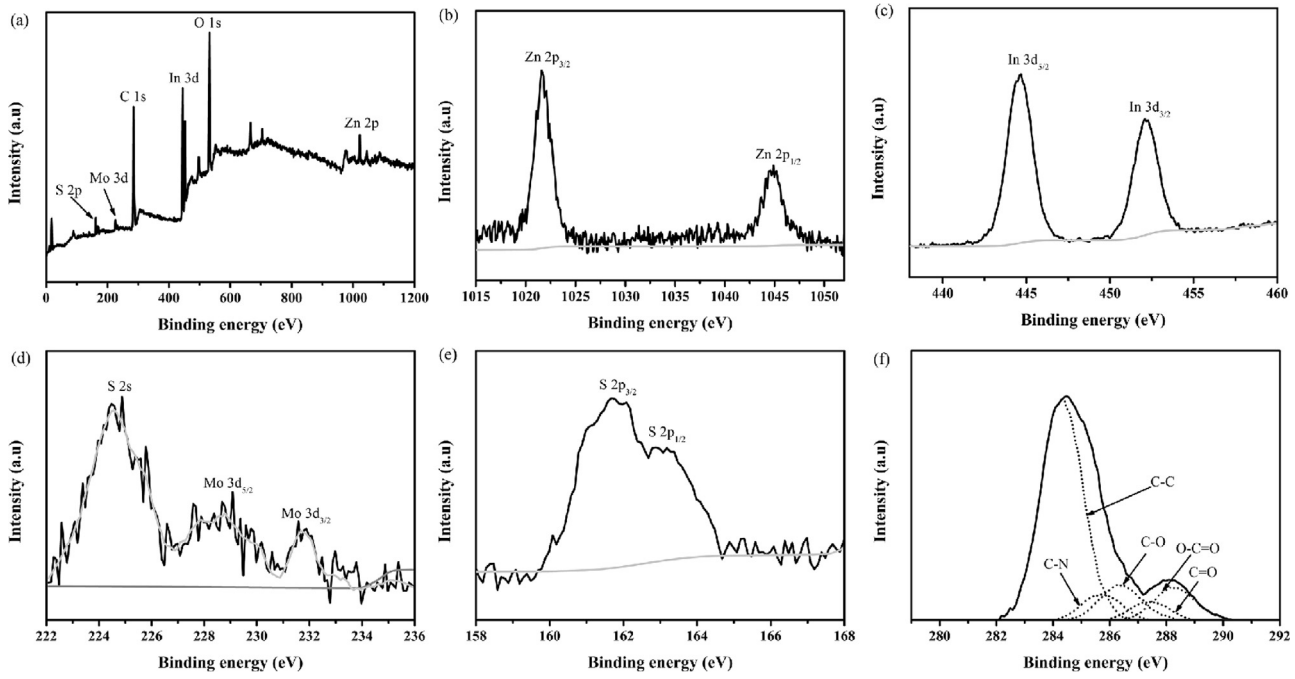

Fig. 4. XPS of 1.2 wt% $Mo_{10}G_1/ZnIn_2S_4$ composite photocatalyst. (a) Survey spectrum, (b) Zn 2p spectrum, (c) In 3d spectrum, (d) Mo 3d spectrum, (e) S 2p spectrum, (f) C 1s spectrum.

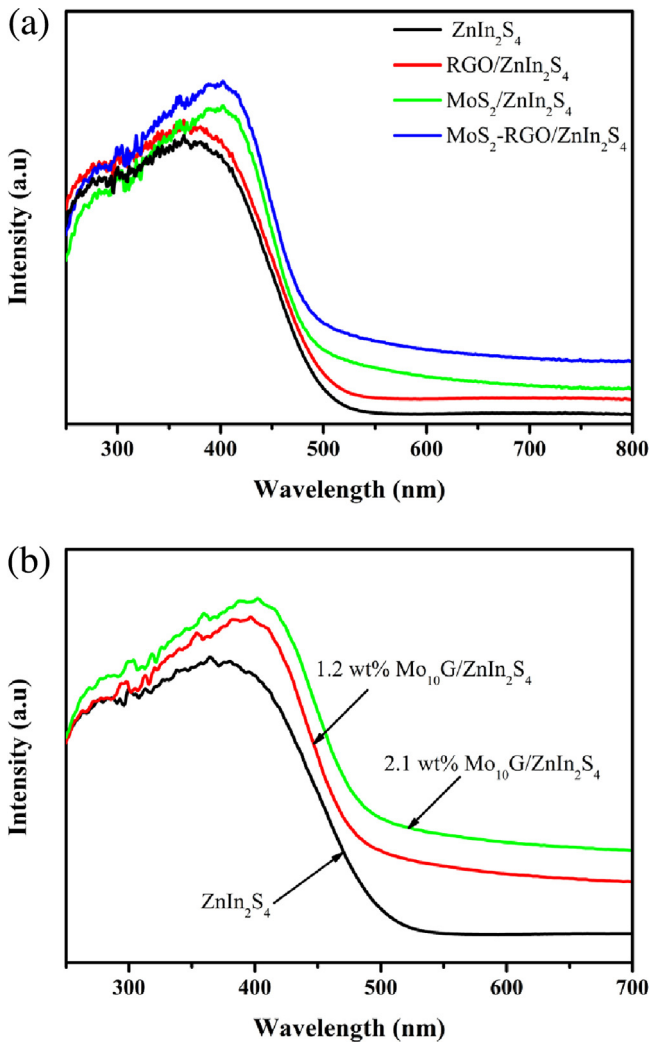

Fig. 5. (a) UV–vis absorption spectra of $ZnIn_2S_4$, 1.2 wt% graphene/$ZnIn_2S_4$, 1.2 wt% MoS_2/$ZnIn_2S_4$ and 1.2 wt% $Mo_{10}G_1$/$ZnIn_2S_4$; (b) UV–vis absorption spectra of $ZnIn_2S_4$, 1.2 wt% $Mo_{10}G_1$/$ZnIn_2S_4$ and 2.1 wt% $Mo_{10}G_1$/$ZnIn_2S_4$.

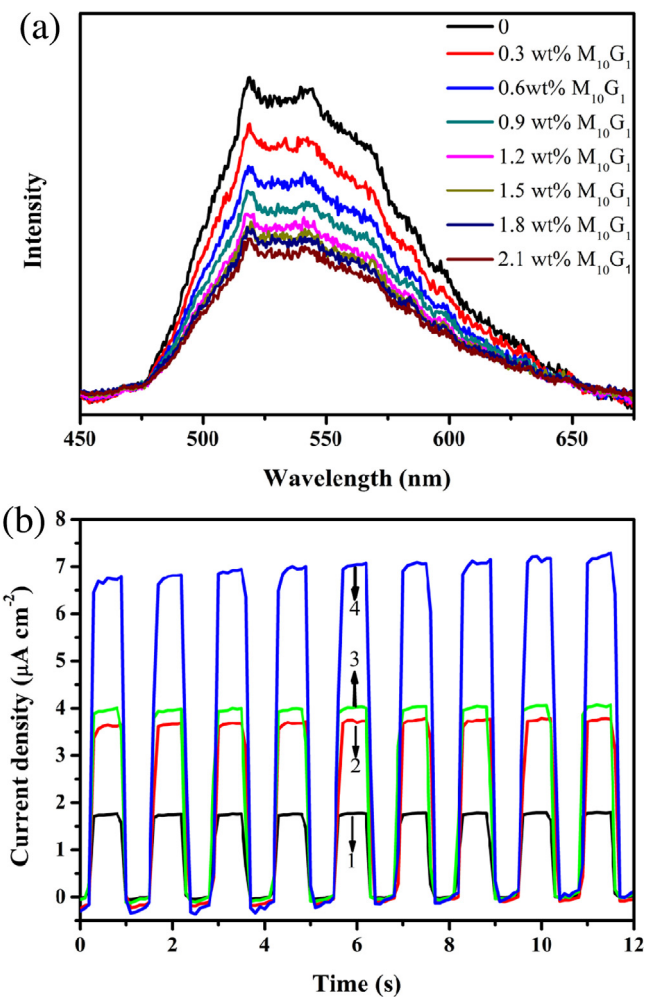

Fig. 6. (a) Comparison of photoluminescence spectra of pure $ZnIn_2S_4$ and $Mo_{10}G_1$/$ZnIn_2S_4$ composites loaded with different amounts of $Mo_{10}G_1$; (b) Transient photocurrent responses of $ZnIn_2S_4$ (1), 1.2 wt% graphene/$ZnIn_2S_4$ (2), 1.2 wt% MoS_2/$ZnIn_2S_4$ (3), and 1.2 wt% $Mo_{10}G_1$/$ZnIn_2S_4$ (4).

$ZnIn_2S_4$ and MoS_2-RGO/$ZnIn_2S_4$ ($Mo_{10}G_1$/$ZnIn_2S_4$) photocatalysts in ethanol solutions (0.5 mg ml^{-1}) excited at 350 nm. All of the samples exhibit a strong emission peak at approximately 530 nm, which can be assigned to the band gap transition of $ZnIn_2S_4$. Remarkably, the intensities of PL spectra for MoS_2/graphene-$ZnIn_2S_4$ decrease with increasing of MoS_2/graphene content, indicating that the recombination of free charge carriers is prevented effectively in the MoS_2/graphene-$ZnIn_2S_4$ composite photocatalysts. That is to say, the excited electrons of $ZnIn_2S_4$ were migrated to MoS_2-RGO cocatalyst for water reduction reaction. In order to further evaluate the transfer efficiency of photogenerated charge carriers, the photocurrent responses of $ZnIn_2S_4$ photoelectrodes loaded with graphene, MoS_2, or MoS_2/graphene were tested since the photocurrent response results from the charge carrier trapping, migration, transfer and separation [45,46]. Fig. 6b shows the periodic on/off photocurrent responses of $ZnIn_2S_4$, graphene/$ZnIn_2S_4$, MoS_2/$ZnIn_2S_4$ and MoS_2/graphene-$ZnIn_2S_4$ photoelectrodes when irradiated under a 300 W Xe lamp equipped with a 420 nm cut-off filter. The unmodified $ZnIn_2S_4$ photoelectrode generated anodic photocurrent with a value of 1.73 μA cm^{-2}. The loading of the graphene and MoS_2 on the surface of $ZnIn_2S_4$ can significantly enhance the photocurrent density for both graphene/$ZnIn_2S_4$ and MoS_2/$ZnIn_2S_4$ photoelectrodes, which show much higher photocurrent densities of 3.59 and 3.94 μA cm^{-2}, respectively. The MoS_2-graphene/$ZnIn_2S_4$ photoelectrode exhibits the highest photocurrent density of 6.98 μA cm^{-2}, which is about 4 times higher than that of $ZnIn_2S_4$ photoelectrode. These results indicate that the MoS_2/graphene composite cocatalyst is a much more active cocatalyst than both MoS_2 and graphene alone to improve the separation efficiency of photogenerated charge carriers in $ZnIn_2S_4$. That is to say, the graphene can act as an electron transport bridge, which accelerates the electron transfer from $ZnIn_2S_4$ to MoS_2 cocatalyst. Similar result has been previously reported in the literatures [35,47,48].

3.2. *Photocatalytic H_2 evolution activity*

Photocatalytic H_2 production experiments were carried out over these as-prepared photocatalysts in the presence of Na_2SO_3 and Na_2S as the sacrificial reagents under visible light irradiation (300 W Xe, λ > 420 nm). Previous report has shown that the optimal loading amount of MoS_2 alone as a cocatalyst to enhance the photocatalytic activity of $ZnIn_2S_4$ is approximately 0.6 wt% [21]. In the present study, 0.6 wt% of MoS_2, graphene, Pt nanoparticles and MoS_2-graphene composite were loaded on the surface of $ZnIn_2S_4$ respectively, and their photocatalytic activities were investigated. As shown in Fig. 7a, the cocatalyst-free $ZnIn_2S_4$ sample has a poor photocatalytic activity with a H_2 evolution rate of 183 μmol h^{-1} g^{-1} under visible light irradiation, which is

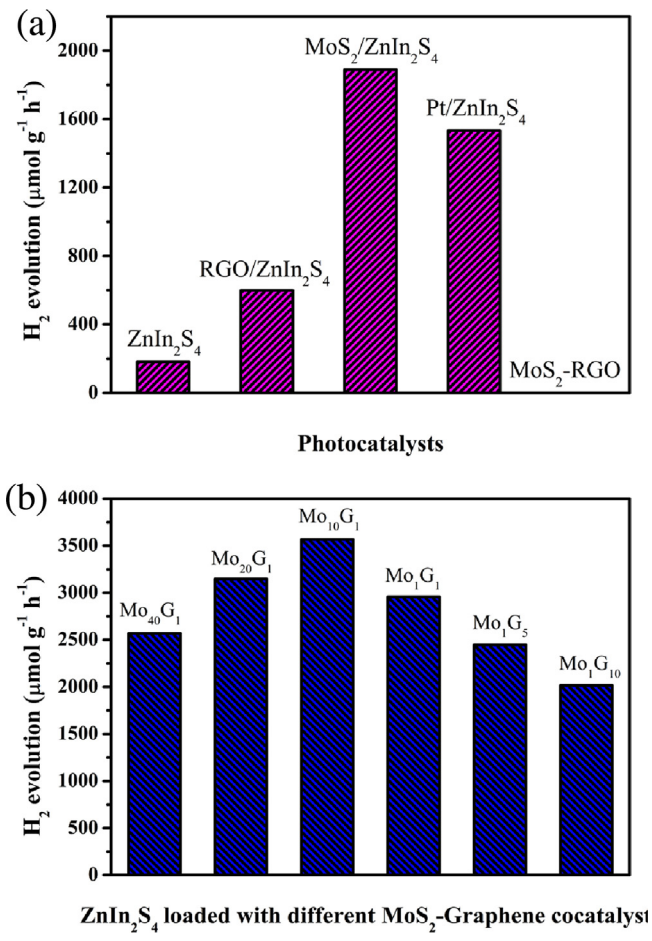

Fig. 7. (a) The rate of H_2 production over $ZnIn_2S_4$ loaded with different cocatalysts (MoS_2-G: MoS_2/Graphene); (b) the rate of H_2 production over $ZnIn_2S_4$ loaded with different MoS_2-graphene cocatalysts. Reaction Conditions: photocatalyst 50 mg; light source, 300 W Xenon lamp equipped with a cut-off filter (λ > 420 nm); Reactant solution, 100 ml aqueous solution containing 0.25 M Na_2S and 0.25 M Na_2SO_3.

result from the fast recombination of photogenerated electron-hole pairs in $ZnIn_2S_4$. The H_2-evolution rates over graphene/$ZnIn_2S_4$ and MoS_2/$ZnIn_2S_4$ photocatalysts are significantly enhanced to 599 and 1889 μmol h^{-1} g^{-1}, which is about 3.3 and 10.4 times of that over pure $ZnIn_2S_4$ photocatalyst under the same conditions, respectively. Although MoS_2-graphene composite has intensive absorption in the ultraviolet and visible regions, no H_2 was observed when it was used as the photocatalyst, indicating that the MoS_2-graphene composite is an inactive photocatalyst for solar H_2 generation [35,36]. More interestingly, as shown in Fig. 7b, a much higher photocatalytic performance was observed when the MoS_2-graphene composite loaded on $ZnIn_2S_4$ surface as a cocatalyst. The catalytic activity of MoS_2-graphene cocatalyst is much higher than both MoS_2 and RGO alone, which can be assigned to the positive synergetic effect between MoS_2 and graphene. In this MoS_2-graphene composite cocatalyst, the MoS_2 and graphene can act as a H_2 evolution reaction catalyst and an electron transport bridge, respectively. The graphene accelerates the electron transfer from the $ZnIn_2S_4$ to MoS_2, which has been demonstrated by the enhanced photocurrent response illustrated in Fig. 6b. The ratio of MoS_2 to graphene in this composite cocatalyst has a significant influence on the photocatalytic activities of MoS_2-graphene/$ZnIn_2S_4$ photocatalysts. To optimize the ratio of MoS_2 to graphene in MoS_2-graphene cocatalysts, the $Mo_{40}G_1$, $Mo_{20}G_1$, $Mo_{10}G_1$, Mo_1G_1, Mo_1G_5 and Mo_1G_{10} composite cocatalysts (for details, see experiment section) were loaded on $ZnIn_2S_4$ surface and their photocatalytic activities for H_2 production were investigated. As shown in Fig. 7b, in presence of a small amount of graphene in the MoS_2-graphene cocatalyst, the H_2 evolution activity of $Mo_{40}G_1$/$ZnIn_2S_4$ photocatalyst was enhanced to 2564 μmol h^{-1} g^{-1}. With expansion of graphene content in MoS_2-graphene cocatalyst, the photocatalytic H_2 evolution activities of MoS_2-graphene/$ZnIn_2S_4$ composites were further enhanced, and the MoS_2-graphene/$ZnIn_2S_4$ photocatalyst with $Mo_{10}G_1$ cocatalyst shows the highest photocatalytic activity with a H_2 evolution rate of 3567 μmol h^{-1} g^{-1}. However, a further increase of graphene content in MoS_2-graphene cocatalyst results in a decreasing H_2 evolution activity. These above results indicate that the catalytic activity of MoS_2-graphene cocatalyst increased remarkably with the increasing ratios of MoS_2 to graphene and then decreased gradually. The enhancement of activities with the increasing ratios of MoS_2 to graphene could be attributed to the increasing density of active sites for hydrogen production reaction. However, a further increase in the ratios of MoS_2 to graphene resulted in decreasing hydrogen production rates, which could be assigned to the decreasing conductivity of photocatalyst for electron transport from $ZnIn_2S_4$ to MoS_2. Similar observation has been encountered in previous studies where the MoS_2-graphene composite was used as a cocatalyst [35,36]. It is well known that the Pt nanoparticles is a highly efficient hydrogen generation reaction catalyst, which has been widely used for solar H_2 evolution [49,50]. For comparsion, the Pt-loaded $ZnIn_2S_4$ photocatalyst was prepared by an *in situ* photodeposition method in H_2PtCl_6 aqueous solution. The Pt/$ZnIn_2S_4$ photocatalyst exhibits a lower photocatalytic activity with a H_2 evolution rate of 1532 μmol h^{-1} g^{-1}. These above results indicate that the MoS_2-graphene composite can act as a more efficient cocatalyst for photocatalytic H_2 evolution production than that of MoS_2, graphene and Pt, and the ratio of graphene to MoS_2 is a key factor in determining the catalytic activity of MoS_2-graphene cocatalyst for solar H_2 generation.

It has been known that the loading amounts of cocatalyst can directly influence the performance of photocatalyst [51–53]. Fig. 8a shows the dependence of the steady rate of H_2 evolution on the amounts of $Mo_{10}G_1$ cocatalyst. The result shows that the H_2 evolution rates increased remarkably with $Mo_{10}G_1$ content to maximum at 1.2 wt%, and then decreased gradually. The 1.2 wt% $Mo_{10}G_1$/$ZnIn_2S_4$ photocatalyst shows the highest H_2 evolution rate of 4167 μmol h^{-1} g^{-1}. Previous research has shown that the H_2 evolution rate catalyzed by a given photocatalyst is enhanced with the increasing amounts of loaded MoS_2-graphene cocatalyst, while excess loading results in decreasing catalytic activity [19,54]. In the present study, when the loading amount of $Mo_{10}G_1$ cocatalyst is less than 1.2 wt%, the H_2 evolution rates increase gradually with the increasing amounts of $Mo_{10}G_1$ cocatalyst, which can be attributed to the increasing density of active sites for H_2 evolution reaction. When the $Mo_{10}G_1$ loading amount exceeded 1.2 wt%, the rates of H_2 evolution decreased gradually with the increasing amounts of $Mo_{10}G_1$. The decreased in photocatalytic H_2 evolution activity is result from the shading effect [36]. That is to say, the introduction of a large of the black MoS_2-graphene cocatalyst can block the absorption of the incident light by the $ZnIn_2S_4$ component. This hypothesis is supported by the absorption spectra of MoS_2-graphene/$ZnIn_2S_4$ photocatalysts illustrated in Fig. 5b.

In addition to the high photocatalytic H_2 evolution activity, the good reusability is another key factor for highly efficient photocatalyst. In order to determine the stability of photocatalyst, the time courses of visible-light-driven H_2 generation over 1.2 wt% $Mo_{10}G_1$/$ZnIn_2S_4$ was evaluated. The cyclic stability of photocatalytic H_2 production reaction with five periods was shown in Fig. 8b. The photocatalytic activity of MoS_2/$ZnIn_2S_4$ photocatalyst did not present any significant loss in the second, third, fourth and fifth cycles, suggesting that the MoS_2/$ZnIn_2S_4$ photocatalyst is stable

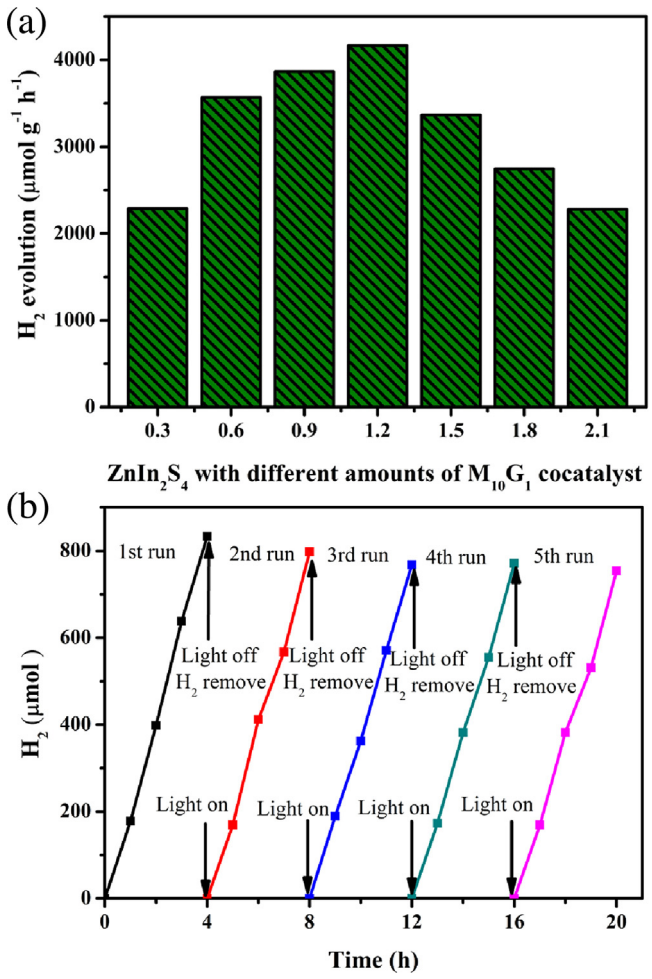

Fig. 8. (a) The rate of H_2 production over $ZnIn_2S_4$ loaded with various amounts of $M_{10}G_1$ cocatalyst; (b) cyclic H_2 production on 1.2 wt% $M_{10}G_1/ZnIn_2S_4$ photocatalyst. Reaction Conditions: photocatalyst 50 mg; light source, 300 W Xenon lamp equipped with a cut-off filter (λ > 420 nm); Reactant solution, 100 ml aqueous solution containing 0.25 M Na_2S and 0.25 M Na_2SO_3.

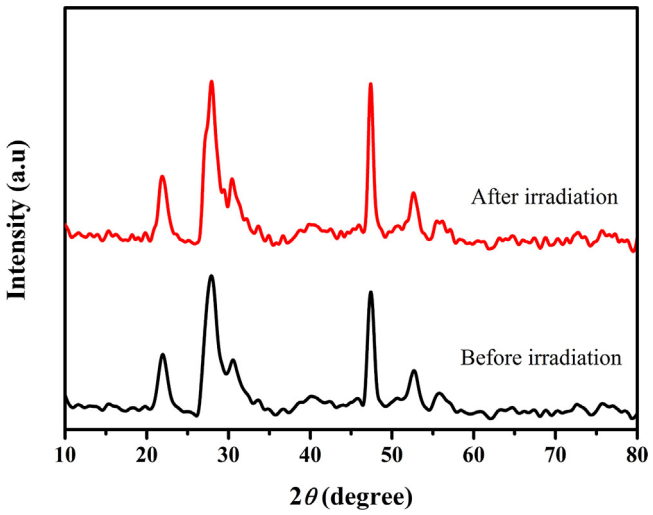

Fig. 9. XRD patterns of 1.2 wt% $Mo_{10}G_1/ZnIn_2S_4$ before and after irradiation.

during the photocatalytic reaction. The total H_2 production after 20 h reaction was 4210 μmol and the H_2 evolution rate after the fifth cycle can keep ca. 91% of the initial rate. This decrease of the H_2 evolution rate from 4169 to 3770 μmol h^{-1} g^{-1} after five cycles could be attributed to the continuous consumption of Na_2S and Na_2SO_3 [36]. In order to confirm this hypothesis, the powder photocatalyst was collected from the H_2 evolution system after three cycles and then characterized by XRD. As shown in Fig. 9, no obvious change in material structure was observed for MoS_2-graphene/$ZnIn_2S_4$ photocatalyst, suggesting that the MoS_2-graphene/$ZnIn_2S_4$ photocatalyst is structurally stable during the photocatalytic water reduction reaction.

Based on above-mentioned observations and results, the tentative mechanism proposed for the superior photocatalytic activity of hierarchical MoS_2-graphene/$ZnIn_2S_4$ photocatalyst is illustrated in Fig. 10a. Under visible light irradiation, the valence band (VB) electrons of $ZnIn_2S_4$ are excited to the conduction band (CB), creating holes in the VB. However, the photogenerated electron-hole pairs can be recombined without cocatalyst loading, resulting in the poor H_2 evolution activity of pure $ZnIn_2S_4$. Previous studies

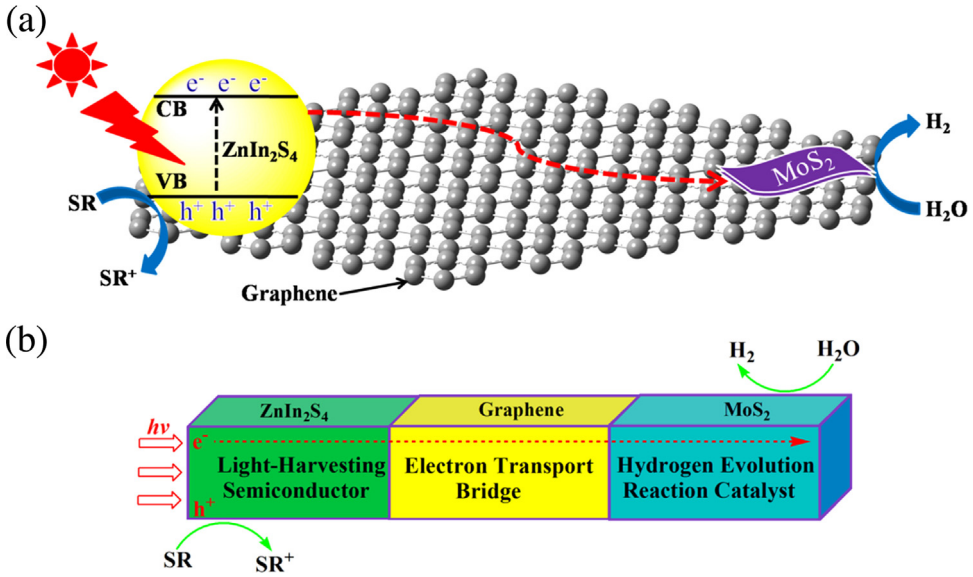

Fig. 10. (a) Schematic illustration for photocatalytic hydrogen generation over MoS_2-graphene/$ZnIn_2S_4$ under visible light irradiation; (b) schematic illustration for charge carriers in MoS_2-graphene/$ZnIn_2S_4$ photocatalyst, $ZnIn_2S_4$: light-harvesting semiconductor, graphene: electron transport bridge, MoS_2: hydrogen evolution reaction catalyst.

have shown that the CB of $ZnIn_2S_4$ is more negative than the graphene/graphene$^{\cdot-}$ ($G/G^{\cdot-}$) redox potential, thus providing the thermodynamic driving force for efficient electron transfer from CB of $ZnIn_2S_4$ to graphene (Fig. S5) [20]. Meanwhile, the $G/G^{\cdot-}$ redox potential is more negative than the CB of MoS_2 nanosheets, providing ample driving force for the electron injection process from the electron-rich graphene$^{\cdot-}$ to the CB of MoS_2 (Fig. 10b) [35]. Finally, the VB of $ZnIn_2S_4$ is more positive than the oxidation potential of sacrificial agents. Thus, the ground $ZnIn_2S_4$ can be reproduced after the hole in the VB was reduced by the sacrificial agents. The superior high photocatalytic activity of MoS_2-graphene/$ZnIn_2S_4$ photocatalyst can be attributed to the synergetic effect between graphene and MoS_2, which includes the suppression of charge carrier recombination, prolongation of charge carrier lifetime, improvement of the interfacial charge transfer and increase in the number of active sites. Transient photocurrent experiments illustrated in Fig. 6b confirm the noticeable improvement in electron transport from $ZnIn_2S_4$ to MoS_2 through the graphene sheets. In addition, there could be little MoS_2 located on the surface of $ZnIn_2S_4$, and some photogenerated electrons can also be transferred directly to the MoS_2 on the surface of $ZnIn_2S_4$, after which reaction with protons to evolve H_2 is possible. However, owing to the high electronic conductivity and high surface area of graphene, the photogenerated electrons of $ZnIn_2S_4$ were mainly transferred to graphene, and then transferred to the MoS_2 for H_2 production.

4. Conclusions

In conclusion, noble-metal-free, visible-light-responsive, environmentally-friendly, highly-reactive and stable MoS_2-graphene/$ZnIn_2S_4$ hierarchical microarchitectures were constructed for robust and effective solar hydrogen evolution. The 1.2 wt% $Mo_{10}G/ZnIn_2S_4$ photocatalyst shows the maximum H_2 evolution rate of 4167 $\mu mol\ h^{-1}\ g^{-1}$ under visible light irradiation, which is nearly 22.8 times higher than that of pure $ZnIn_2S_4$. More importantly, the MoS_2-graphene/$ZnIn_2S_4$ exhibits much higher activity than that of Pt-loaded $ZnIn_2S_4$ under the same conditions, indicating that the two-dimensional MoS_2-graphene composite can act as a more effective cocatalyst than the commonly used Pt. The superior photocatalytic H_2 production activity of the MoS_2-graphene/$ZnIn_2S_4$ photocatalyst could be ascribed to the positive synergetic effect between MoS_2 and graphene in MoS_2-graphene composite cocatalyst, in which the MoS_2 and graphene act as a hydrogen evolution reaction catalyst and electron transfer bridge, respectively. This study provides a new noble-metal-free, visible-light-responding, environmentally-friendly, highly-efficient and stable system in the development of graphene-based photocatalysts for solar hydrogen generation.

Acknowledgments

This work was financially supported by the National Natural Science Foundation of China (No. 51502068, 21271170 and 51572065), the Natural Science Foundation of Zhejiang Province (No. LQ16B030002), the Natural Science Foundation of Zhejiang Province for Distinguished Young Scholars (LR15E020001) and the National Basic Research Program of China (No. 2013CB632404).

Appendix A. Supplementary data

Supplementary data associated with this article can be found, in the online version, at http://dx.doi.org/10.1016/j.apcatb.2016.01.061.

References

[1] N.S. Lewis, D.G. Nocera, Proc. Natl. Acad. Sci. U. S. A. 103 (2006) 15729–15735.
[2] H. Tong, S.X. Ouyang, Y.P. Bi, N. Umezawa, M. Oshikiri, J.H. Ye, Adv. Mater. 24 (2012) 229–251.
[3] A. Kudo, Y. Miseki, Chem. Soc. Rev. 38 (2009) 253–278.
[4] S. Obregón, M.J. Muñoz-Batista, M. Fernández-García, A. Kubacka, G. Colóna, Appl. Catal. B: Environ. 179 (2015) 468–478.
[5] Y. Ma, X.L. Wang, Y.S. Jia, X.B. Chen, H.X. Han, C. Li, Chem. Rev. 114 (2014) 9987–10043.
[6] J.X.B. Chen, S.H. Shen, L.J. Guo, S.S. Mao, Chem. Rev. 110 (2010) 6503–6570.
[7] Y.F. Zhao, Z.Y. Yang, Y.X. Zhang, L. Jing, X. Guo, Z.T. Ke, P.W. Hu, G.X. Wang, Y.M. Yan, K.N. Sun, J. Phys. Chem. C 118 (2014) 14238–14245.
[8] L.J. Shen, M.B. Luo, Y.H. Liu, R.W. Liang, F.F. Jing, L. Wu, Appl. Catal. B: Environ. 166–167 (2015) 445–453.
[9] H.J. Yan, J.H. Yang, G.J. Ma, G.P. Wu, X. Zong, Z.B. Lei, J.Y. Shi, C. Li, J. Catal. 266 (2009) 165–168.
[10] X.W. Wang, G. Liu, L.Z. Wang, Z.G. Chen, G.Q. Lu, H.M. Chen, Adv. Energy Mater. 2 (2012) 42–46.
[11] Z.J. Li, J.J. Wang, X.B. Li, X.B. Fan, Q.Y. Meng, K. Feng, B. Chen, C.H. Tung, L.Z. Wu, Adv. Mater. 25 (2013) 6613–6618.
[12] L. Zheng, Y. Xu, Y. Song, C.Z. Wu, M. Zhang, Y. Xie, Inorg. Chem. 48 (2009) 4003–4009.
[13] E. Ha, L.Y.S. Lee, J.C. Wang, F.H. Li, K.Y. Wong, S.C.E. Tsang, Adv. Mater. 26 (2014) 3496–3500.
[14] K. Maeda, D.L. Lu, K. Domen, Chem. Eur. J. 19 (2013) 4986–4991.
[15] K. Maeda, K. Domen, J. Phys. Chem. C 111 (2007) 7851–7861.
[16] X.C. Wang, K. Maeda, A. Thomas, K. Takanabe, G. Xin, J.M. Carlsson, K. Domen, M. Antonietti, Nat. Mater. 8 (2009) 76–80.
[17] S.H. Shen, L. Zhao, Z.H. Zhou, L.J. Guo, J. Phys. Chem. C 112 (2008) 16148–16155.
[18] B. Chai, T.Y. Peng, P. Zeng, X.H. Zhang, Dalton. Trans. 41 (2012) 1179–1186.
[19] Z.B. Lei, W.S. You, Mei Y. Liu, G.H. Zhou, T. Takata, M. Hara, K. Domen, C. Li, Chem. Commun. (2003) 2142–2143.
[20] J.L. Ye, Z. Xu, R.S. Yuan, Z.H. Li, ACS Appl. Mater. Interfaces 6 (2014) 3483–3490.
[21] L. Wei, Y.J. Chen, Y.B. Lin, H.S. Wu, R.S. Yuan, Z.H. Li, Appl. Catal. B. Environ. 144 144 (2014) 521–527.
[22] W.J. Zhou, Z.Y. Yin, Y.P. Du, X. Huang, Z.Y. Zeng, Z.X. Fan, H. Liu, J.Y. Wang, H. Zhang, Small 9 (2013) 140–147.
[23] Y.J. Yuan, H.W. Lu, Z.T. Yu, Z.G. Zou, ChemSusChem 8 (2015) 4113–4127.
[24] J. Kibsgaard, Z.B. Chen, B.N. Reinecke, T.F. Jaramillo, Nat. Mater. 11 (2012) 963–969.
[25] Y.G. Li, H.L. Wang, L.M. Xie, Y.Y. Liang, G.S. Hong, H.J. Dai, J. Am. Chem. Soc. 133 (2011) 7296–7299.
[26] J.D. Benck, T.R. Hellstern, J. Kibsgaard, P. Chakthranont, T.F. Jaramillo, ACS Catal. 4 (2014) 3957–3971.
[27] C.B. Liu, L.L. Wang, Y.H. Tang, S.L. Luo, Y.T. Liu, S.Q. Zhang, Y.X. Zeng, Y.Z. Xu, Appl. Catal. B. Environ. 144 (2015) 1–9.
[28] H. Sabbah, L. Biennier, I.R. Sims, Y. Georgievskii, S.J. Klippenstein, I.W.M. Smith, Science 317 (2007) 100–102.
[29] M.Q. Yang, C. Han, Y.J. Xu, J. Phys. Chem. C 119 (2015) 27234–27246.
[30] X. Zong, H.J. Yan, G.P. Wu, G.J. Ma, F.Y. Wen, L. Wang, C. Li, J. Am. Chem. Soc. 130 (2008) 7176–7177.
[31] Y.D. Hou, A.B. Laursen, J.S. Zhang, G.G. Zhang, Y.S. Zhu, X.C. Wang, S. Dahl, I. Chorkendorff, Angew. Chem. Int. Ed. 52 (2013) 3621–3625.
[32] Y.J. Yuan, F. Wang, B. Hu, H.W. Lu, Z.T. Yu, Z.G. Zou, Dalton. Trans. 44 (2015) 10997–11003.
[33] M.Q. Yang, N. Zhang, M. Pagliaro, Y.J. Xu, Chem. Soc. Rev. 43 (2014) 8240–8254.
[34] N. Zhang, M.Q. Yang, S. Liu, Y. Sun, Y.J. Xu, Chem. Rev. 115 (2015) 10307–10377.
[35] Q.J. Xiang, J.G. Yu, M. Jaroniec, J. Am. Chem. Soc. 134 134 (2012) 6575–6578.
[36] K. Chang, Z.W. Mei, T. Wang, Q. Kang, S.X. Ouyang, J.H. Ye, ACS Nano 8 (2014) 7078–7087.
[37] K. Chang, W. Chen, ACS Nano 28 (2011) 4720–4728.
[38] J. Xiao, X.J. Wang, X.Q. Yang, S.D. Xun, G. Liu, P.K. Koech, J. Liu, J.P. Lemmon, Adv. Funct. Mater. 9 (2011) 2840–2846.
[39] L. Ge, C.C. Han, X.L. Xiao, L.L. Guo, Int. J. Hydrogen Energy 38 (2013) 6960–6969.
[40] F. Meng, J.T. Li, S.K. Cushing, M.J. Zhi, N.Q. Wu, J. Am. Chem. Soc. 135 (2013) 10286–10289.
[41] U. Maitra, U. Gupta, M. De, R. Datta, A. Govindaraj, C.N.R. Rao, Angew. Chem. Int. Ed. 52 (2013) 13057–13061.
[42] N.S. Chaudhari, A.P. Bhirud, R.S. Sonawane, L.K. Nikam, S.S. Warule, V.H. Rane, B.B. Kale, Green Chem. 13 (2011) 2500–2506.
[43] T.F. Yeh, C.Y. Teng, S.J. Chen, H. Teng, Adv. Mater. 26 (2014) 3297–3303.
[44] J.H. Yang, D.E. Wang, H.X. Han, C. Li, Acc. Chem. Res. 46 (2013) 1900–1909.
[45] J.G. Yu, L.F. Qi, M. Jaroniec, J. Phys. Chem. C 114 (2010) 13118–13125.
[46] Y.L. Min, G.Q. He, Q.J. Xu, Y.C. Chen, J. Mater. Chem. A 2 (2014) 2578–2584.
[47] Q.J. Xiang, J.G. Yu, J. Phys. Chem. Lett. 4 (2013) 753–759.
[48] Q.J. Xiang, B. Cheng, J.G. Yu, Angew. Chem. Int. Ed. 54 (2015) 11350–11366.
[49] Q. Li, B.D. Guo, J.G. Yu, J.R. Ran, B.H. Zhang, H.J. Yan, J.R. Gong, J. Am. Chem. Soc. 133 (2011) 10878–10884.
[50] Y.Z. Yang, C.H. Chang, H. Idris, Appl. Catal. B. Environ. 67 (2006) 217–222.

[51] K. Maeda, X. Wang, Y. Nishihara, D. Lu, M. Antonietti, K. Domen, J. Phys. Chem. C 113 (2009) 4940–4947.
[52] Z.P. Yan, X.X. Yu, A.L. Han, P. Xu, P.W. Du, J. Phys. Chem. C 118 (2014) 22896–22903.
[53] Y.J. Yuan, Z.J. Ye, H. Lu, B. Hu, Y.H. Li, D.Q. Chen, J.S. Zhong, Z.T. Yu, Z.G. Zou, ACS Catal. 6 (2016) 532–541.
[54] Y.J. Yuan, Z.T. Yu, Y.H. Li, H.W. Lu, X. Chen, W.G. Tu, Z.G. Ji, Z.G. Zou, Appl. Catal. B. Environ. 181 (2016) 16–23.